Chapter

Aerodynamics of Mars 2020 Rover Wind Sensors

Rafael Bardera, Suthyvann Sor and Adelaida García-Magariño

Abstract

Environmental factors in Mars atmosphere are a part of the research issues of the future Mars 2020 mission. The new rover surface vehicle will transport different instruments to investigate the geology, biology, and meteorology of Mars. Amongst these instruments, the Mars Environmental Dynamics Analyzer (MEDA) will be dedicated to the measurement of environment parameters. Two wind sensors will be included in the meteorological station MEDA because wind plays a very important role in Martian climate. High-quality wind data are required to build mathematical models of the Mars climate; therefore, powerful techniques are necessary to eliminate aerodynamic perturbations produced by the rover presence over wind measurements. This chapter is dedicated to the characterization of the aerodynamics around the Mars 2020 rover and its interaction with the rover Mars surface vehicle in order to get information to correct wind data coming from Mars.

Keywords: aerodynamics, rover, Mars, wind, sensors

1. Introduction

The Mars 2020 rover mission is a part of NASA's Mars Exploration Program. This mission is conceived for the exploration of Mars, and additionally, it provides a way to demonstrate novel technologies addressed to the future Martian human expeditions [1]. The investigation of the environmental factors is an overriding aspect to get insight and a better understanding of the meteorological processes in Mars atmosphere. Satellites orbiting Mars provide remote sensing data for the study of Martian atmosphere, but a higher resolution data must be obtained by means of investigation surface vehicles.

The Mars Environmental Dynamics Analyzer (MEDA) is the contribution of Spain to the Mars Exploration Program, and it was designed as a mobile environmental station to be transported by Mars 2020 rover. MEDA sensors will provide information about both ambient and ground, such as wind speed and its direction, temperature, pressure, relative humidity, ultraviolet radiation, and size and shape of dust. MEDA wind sensors are inspired in the design of the wind sensor of Rover Environmental Monitoring Station (REMS) [2, 3] that was embarked on the Mars Science Laboratory (MSL) Curiosity rover [4].

The importance of studying the wind in Mars is manifold. On one hand, in situ propulsion will be necessary for long-term planetary surface missions, and the wind energy could be the power to push wind-driven craft for exploration. On the other

hand, quality measurements of the wind in Mars could provide a better understanding of the geophysical phenomena occurring in Mars such as dust devils, carving intracrater layered deposits, and changes on dunes or any other eolian processes due to the wind-driven particle mobility.

2. The Mars atmosphere

The Martian atmosphere is mainly composed of CO2 (95.3%), with small amounts of Nitrogen and other gases. Typical surface atmosphere conditions are a pressure of 700 Pa [5] and a surface temperature variable in the range from 145 to 245 K [6]. The atmosphere density ρ can be calculated considering the perfect gases law as follows:

$$\rho_{Mars} = \frac{P}{R_g T} = \frac{700}{188.918 \times 195} = 0.019\ kg/m^3 \tag{1}$$

where R_g is the constant of CO2 gas taken as $RCO2$ = 188.918 J/kg·K, and T is the mean temperature in Kelvin degrees. The result indicates that the Mars atmosphere density is very low compared with the Earth atmosphere ($\rho_{Earth} = 65\rho_{Mars}$). When the density of a flow is very low, as is this case, usually, the hypothesis of continuum media is investigated by means of the nondimensional Knudsen number (Kn), given by,

$$Kn = \frac{\lambda}{L} \tag{2}$$

where λ is the mean free path, related with the averaged distance between nearest molecules of the gas, and L is a characteristic length scale of the fluidic system or process under study. Although the mean free path depends on the temperature and pressure conditions, a typical value for Mars atmosphere is of order of 10 μm. On the other hand, the typical length of the process can be taken as the characteristic length of rover vehicle ($L \sim 1.7$ m). When analyzing the local flow over rover wind sensors, the boom diameter ($L \sim 0.05$ m) must be taken, resulting in last case, a Knudsen number of order of $2 \times 10^{-4} << 0.1$, [7] and consequently, the gas of Mars atmosphere can be considered as a continuous media.

On the other hand, the dynamic viscosity (μ) in standard Mars conditions can be computed following the Sutherland law [8]:

$$\mu(T) = \mu_0 \left(\frac{T}{T_0}\right)^{3/2} \left(\frac{T_0 + S}{T + S}\right) \tag{3}$$

where T_0 = 273 K, S = 222 K, and μ_0 is the dynamic viscosity at T_0, taken as $\mu_0 = 1.37 \times 10^{-5}$ N·s/m^2. Computation of Eq. (3) gives a dynamic viscosity coefficient value $\mu = 9.817 \times 10^{-6}\text{N} \cdot \text{s}/m^2$ when temperature is 195 K.

Finally, kinematic viscosity coefficient (ν) is given by the ratio of the dynamic viscosity to gas density ($\nu = \mu/\rho$) resulting a value of 5.167×10^{-4} m^2/s. **Table 1** shows the main Mars atmosphere parameters compared with Earth values, including the Mars gravity being 3.7 m/s^2.

From the aerodynamics point of view, the most important parameter to evaluate incompressible flows is the Reynolds number (Re), which is a dimensionless parameter defined as the ratio of inertial forces ($\sim \rho V^2 L$) to viscous forces ($\sim \mu V/L^2$) and also indicates how turbulent the flow is. The expression of Reynolds number is as follows:

parameter	symbol	units	Mars	Earth
Pressure	P	Pa	700	101300
Temperature	T	K	195	288
Density	ρ	kg/m^3	0,019	1,225
Dynamic viscosity	μ	N·s/m^2	9,82×10^{-6}	1,79 ×10^{-5}
Kinematic viscosity	ν	m^2/s	5,17×10^{-4}	1,46 ×10^{-5}
Gravity	g	m/s^2	3,7	9,8

Table 1.
Typical atmosphere flow conditions in Mars compared with Earth.

$$Re = \frac{VL}{\nu} \tag{4}$$

where V is the flow velocity, L a typical length, and ν the kinematic viscosity coefficient of the fluid.

Additionally, Reynolds number is a fundamental parameter that satisfies the dynamic similarity, which is necessary to maintain the similarity between both aerodynamic flows, in Mars and in Earth. The Reynolds ratio is given by

$$\frac{Re_{Earth}}{Re_{Mars}} = \frac{V_{Earth}L_{Earth}}{V_{Mars}L_{Mars}}\frac{\nu_{Mars}}{\nu_{Earth}}. \tag{5}$$

Thereby, when a wind is blowing, in both planets, with the same velocity V over the same object with a characteristic length L, different Reynolds numbers are obtained, and the Reynolds ratio only depends on the physical atmosphere properties, such as kinematic viscosity, which is related to thermodynamics conditions (P and T) so that, in this case, the Reynolds similarity law is conversely proportional to the corresponding kinematic viscosity coefficient

$$\frac{Re_{Earth}}{Re_{Mars}} = \frac{\nu_{Mars}}{\nu_{Earth}} = 35.4. \tag{6}$$

Consequently, the Reynolds number in Earth is approximately 35 times higher than these to be expected in Mars surface, when Earth conditions corresponds to standard atmospheric conditions; therefore, Reynolds in Earth only can be equal when using same gas and same thermodynamics conditions as those present in Mars. But, if we are trying to simulate the problem by wind tunnel testing in Earth atmospheric conditions, flow velocity and length in Earth will be reduced in the same quantity of kinematic viscosity ratio, in order to verify the same Reynolds number in both planets. Because velocity can be slightly reduced, but length can be modified in a large range, this way will be followed by wind tunnel testing. For example, an experiment of the same velocity requires a subscaled model of 1/35th scale, while a reduction to 1/2 of flow velocity requires a reduction of approximately 1/18th in all dimensions of the rover model to be tested in Earth.

3. The Mars 2020 rover

Mars 2020 rover is a nuclear-powered ground vehicle that transports a set of scientific instruments dedicated to investigate the Martian surface. The rover is

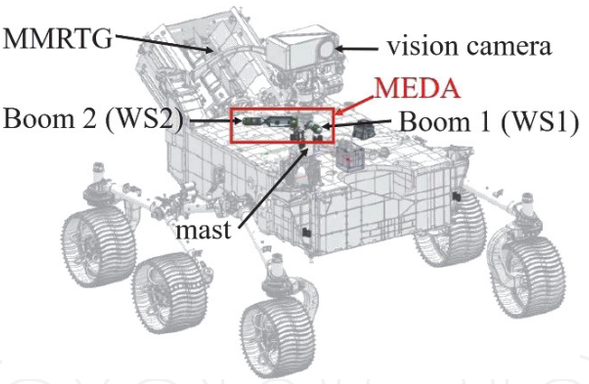

Figure 1.
Scheme of the Mars rover vehicle.

basically composed of a central box body with rectangular section supported by six wheels. A vertical mast supports the remote vision camera and MEDA environmental instruments and an articulated robotic arm is dedicated to get biologic and geologic samples from soil.

Electrical power for engineering systems and science payload of the rover is provided by the Multi-Mission Radioisotope Thermoelectric Generator (MMRGT). The MMRGT converts heat from the natural radioactive plutonium into electrical power [1]. MMRGT is a cylindrical box connected to heat dissipation fins and two heat exchanger plates [9]. **Figure 1** shows a general view of the Mars 2020 rover vehicle (robotic arm was not represented for a better vision of the rover devices).

MEDA wind sensors are located in both booms, around the Remote Sensing Mast (RSM) and oriented 120° from each other. Sensors are capable to measure wind speed up to 70 m/s, and they are located on the rover mast and affected by the rover presence. A correction of the wind data is necessary in order to obtain correct measurements by avoiding the flow perturbation produced by the rover.

4. Thermal anemometry

Thermal anemometry, usually named as hot wire (HW) technique, is a well-established measurement technique introduced in the first half of twentieth century from the study carried out by King after investigating the thin cylinders heat transfer. This technique has got a very high state of development, offering high quality in measuring flow velocities and especially for study of turbulent flows. Air flow velocity and fluctuations can be measured by HW based on the detection of rapid changes in the transferred heat from a tiny sensor (wire typically 5 μm in diameter) to the flow. This sensor is electrically heated so that the flow velocity is determined from the electric power necessary to maintain the temperature of wire at a constant value, by means of an electronic circuit that provides an automatic control loop of temperature. This type of HW is named as Constant Temperature Anemometer (CTA). When electric current crosses through the wire, its temperature is rising due to the heat produced by Joule effect. In a stationary situation, the heat produced is equilibrated by the refrigeration effect produced by the gas flow motion. The energy variation of the wire is given by the following expression:

$$\frac{dE}{dt} = \frac{dW}{dt} + \frac{dQ}{dt} \tag{7}$$

where E is the energy of the wire, Q is the transferred heat to the flow, and W is the heating power, related with the electric intensity I and the resistance of the wire R, given by

$$\frac{dW}{dt} = I^2R \tag{8}$$

On the other hand, the convicted heat is given by the Newton's cooling law as follows:

$$\frac{dQ}{dt} = h(T_w - T_\infty)A_w \tag{9}$$

where h is the thermal convection coefficient, T_w is the wire temperature, T_∞ is the flow temperature, and A_w is the area of heat transfer for the wire.

Dimensional analysis indicates that thermal convection coefficient depends on the conductivity of fluid k, wire diameter d, and the Nusselt number so that

$$h = \frac{k}{d}Nu \tag{10}$$

where Nu is the nondimensional Nusselt number that represents the convection heat transfer to the conduction heat transfer ratio.

Assuming the orientation of the wire as constant, low airspeed, natural convection is neglectable, and Prandtl number as constant as usual in gases flows, the Nusselt number is only a function of the Reynolds number Re

$$Nu = Nu(Re). \tag{11}$$

This function was empirically determined by King, as the following potential correlation:

$$Nu = C + D\,Re^n. \tag{12}$$

So that, the output signal measured between the ends of the wire is the square of voltage E_W^2 related with wind velocity as follows:

$$E_W^2 = I^2R^2 = (C_1 + D_1U^n)(T_w - T_\infty) \tag{13}$$

where coefficients C_1, D_1, and n must be experimentally determined by calibration.

Concluding, the voltage E_W is a measurement directly related with the flow velocity.

5. Rover wind sensors

Several wind sensors are described in the literature [8]. Some sensors based on flow dynamic pressure (Pitot-static probe, rotating sensors as cup and vane anemometers, etc.) were discarded to be used in Mars, mainly due to the very low density of Martian atmosphere, and others as Laser Doppler Anemometry (LDA) because they require an appropriate particle seeding of the flow. Finally, thermal anemometry was selected because it offers reliability in a wide range of temperature, simplicity and robustness, low power consumption, high resolution, and short time of response [4]. Moreover, this technology was used during the Viking mission, demonstrating their measurement capabilities in the Martian atmosphere [10, 11].

MEDA wind sensors are a new design based on the wind REMS sensor [2, 3] that was embarked on the Mars Science Laboratory (MSL) Curiosity rover [4] currently sending data from Mars atmosphere. The behavior of thermal wind sensors installed over the boom of the Mars rover is similar to hot wire, described in earlier paragraph. They are based on a group of four sensitive surface hot film sensors (named dices A, B, C, and D) installed in the same plane (see **Figure 2**). Sensors are refrigerated when the wind is blowing over each dice, and consequently, an electric power must be apply to keep temperature constant on the dice (constant operation reference temperature CTA). The value of electric power gives a measurement of the airspeed on each dice and the direction from blowing. Dices situated in front the flow are cooled more than those located in back positions, since the wind heats up as the first ones are cooled and heat is transferred to the airstream. A comparative analysis of the electric power required for each of the four dices will give us an indication of the angle of incidence of the air flow.

Finally, a joint calibration of the four dices allows us to know the wind speed and the incidence angle over the sensor. A more detailed description is in Ref. [4].

Figure 3 shows the set-up for functional tests of rover wind sensors. A simplified version of hot film sensor, similar to the real sensor was implemented over a flat plate. A specially designed bed fabrication in extruded polystyrene was used to support the plate with hot film sensors in order to perform the functional tests by wind tunnel testing to verify the wind endurance. During this test campaign, several values of airspeed were blown by wind tunnel and the air was flowing on the sensors refrigerating them. Readings of electric signals from dices electronic chip were acquired to verify the correct behavior of the wind sensors, and its integrity was verified when the flow was blowing over them. A laser Doppler anemometer was used as an airspeed standard.

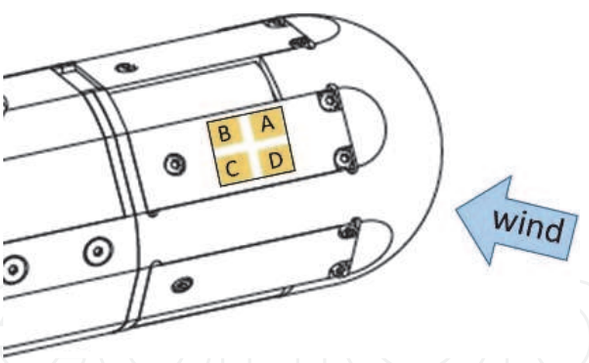

Figure 2.
Rover wind sensor boom.

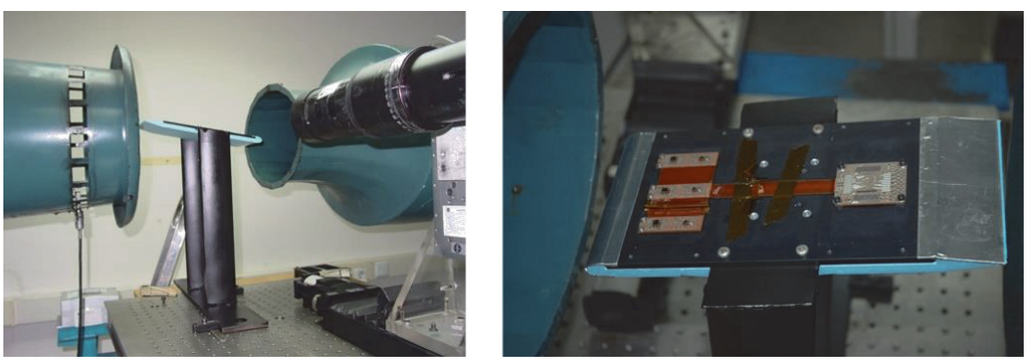

Figure 3.
Mars rover wind sensors during functional tests.

6. Boom aerodynamics

The rover wind sensors are installed on the boom surface. Booms are located in the vertical mast over the upper rover central box surface (see **Figures 1** and **2**). Two booms are at the same height and contained in the same horizontal plane, with an angular offset of 120°. The boom external geometry is similar to these of the Pitot-static tube. This is a classical instrument for measuring airspeed in aerodynamics and fluid mechanics that has proven its efficiency for more than a century. This tube has a hemispherical head followed by a cylindrical body with axisymmetric geometry so that the longitudinal flow is coming to the wind sensor without detachment. On the other hand, rover booms have a hemispherical head followed by a cylindrical body with polygonal faces where thermal sensors are installed (see **Figure 2**). In this section, a theoretical analysis of two simplified cases is presented: longitudinal axisymmetric flow and cross flow over the boom.

6.1 Longitudinal axisymmetric flow

When the wind is blowing in longitudinal axisymmetric direction, the head of the boom receives the flow without detachment. A first approximation to this kind of flow can be studied by considering the incompressible potential flow on the axisymmetric Rankine half-body of revolution. This flow is produced when a uniform stream of velocity U_∞ is flowing over a three-dimensional point source of strength M located at the origin. This situation is depicted in **Figure 4**, for a half-body of revolution with radius a.

A stagnation point denoted by P is produced by the upstream source point when both singularities are equal in velocity. The location of this point is calculated as follows:

$$U_\infty = \frac{M}{4\pi d^2}, \tag{14}$$

and finally, the distance to point P is

$$d = \frac{1}{2}\sqrt{\frac{M}{\pi U_\infty}}. \tag{15}$$

The velocity potential Φ corresponding to the superposition of a uniform stream and a source located in the origin is given by the following expression:

$$\Phi(\mathrm{x}, \mathrm{r}) = U_\infty x - \frac{M}{4\pi R} \tag{16}$$

where $R = \sqrt{x^2 + r^2}$.

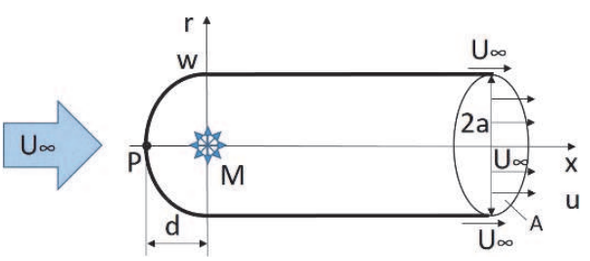

Figure 4.
Axial flow over wind sensor boom.

On the other hand, the Stokes stream function Ψ for this flow is given by,

$$\Psi(r,z) = \frac{M}{2}\left(1 - \frac{x}{R}\right) + \pi r^2 U_\infty. \tag{17}$$

The half-body surface stream function is equal to the flow rate coming from the inner of the half-body. Taking into account that it is a body of revolution, transversal area is $A = \pi a^2$ and the flow coming from the inner body, crossing the circular area denoted as A (see **Figure 4**), is AU_∞, exactly the strength of the point source ($M = \pi a^2 U_\infty$), and the distance d is computed being $d = a/2$.

The dividing streamline represents the surface body, and it is obtained when the stream function is equal to the source strength, M,

$$M = \frac{M}{2}\left(1 - \frac{x}{R}\right) + \pi r^2 U_\infty. \tag{18}$$

And the corresponding velocity is

$$u(x,r) = \frac{\partial \Phi(x,r)}{\partial x} = U_\infty + \frac{M}{4\pi}\frac{x}{\left(x^2 + r^2\right)^{3/2}} \tag{19}$$

$$w(x,r) = \frac{\partial \Phi(x,r)}{\partial r} = \frac{M}{4\pi}\frac{r}{\left(x^2 + r^2\right)^{3/2}}. \tag{20}$$

Velocity over body surface is computed taking into account that both variables x and r are related by the body stream function as follows:

$$\frac{M}{2}\left(1 + \frac{x}{R}\right) = \pi r^2 U_\infty \tag{21}$$

Resulting in

$$r^2 = \frac{a^2}{2}\left(1 + \frac{x}{\sqrt{x^2 + r^2}}\right) \tag{22}$$

Taking nondimensional variables defined as

$$\chi = \frac{x}{2a} \tag{23}$$

$$\zeta = \frac{r}{2a}. \tag{24}$$

Both variables are related by the stream function as follows:

$$8\zeta^2 = 1 + \frac{\chi}{\sqrt{\chi^2 + \zeta^2}}. \tag{25}$$

The variable χ results in a function of ζ, given by,

$$\chi^2 = \frac{\left(8\zeta^2 - 1\right)^2}{16\left(1 - 4\zeta^2\right)}. \tag{26}$$

Finally, the longitudinal velocity component is given by the following expression:

$$\frac{u(x,r)}{U_\infty} = 1 + \frac{1}{16}\frac{\chi}{\sqrt{\left(\chi^2+\zeta^2\right)^3}}. \tag{27}$$

And simplifying, we can find an expression that only depends on the unique variable, ζ, as follows:

$$\frac{u(x,r)}{U_\infty} = 1 + \frac{\left(8\zeta^2-1\right)\sqrt{\left(1-4\zeta^2\right)}}{64}. \tag{28}$$

Figure 5 shows the graph of nondimensional velocity u/U_∞ versus the nondimensional distance $x/2a$. The velocity is growing from the stagnation point located at $\chi_P = -1/4$ until unity nondimensional velocity that is reached when curve cross the origin ($\chi = 0$). After that, a peak is produced, and the freestream velocity value is got for a longitudinal distance $x/2a = 1.5$. So that, when the flow is coming to a boom section located at a distance of approximately equal to three times the radius ($x = 3a$), the wind flows with the freestream velocity, and the hot film sensor will be refrigerated by the same manner as in nonperturbed conditions.

6.2 Transversal flow

Wind flowing transversal to the boom (boom in cross-flow) can be studied as a first approximation by the two-dimensional complex potential flow over a circular cylinder, as represented in **Figure 6**.

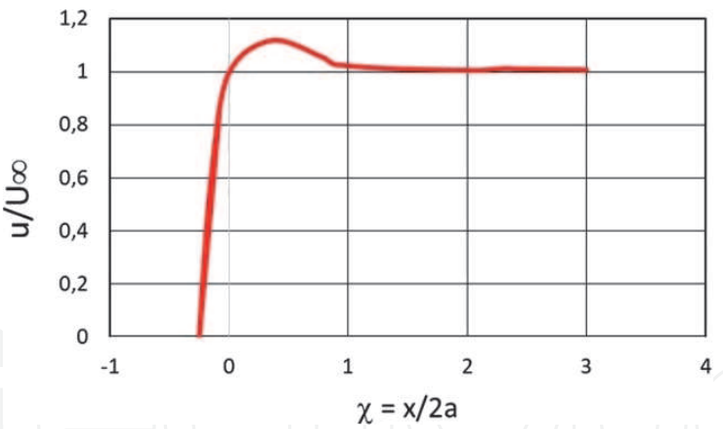

Figure 5.
Nondimensional wind velocity on rover boom in axial flow.

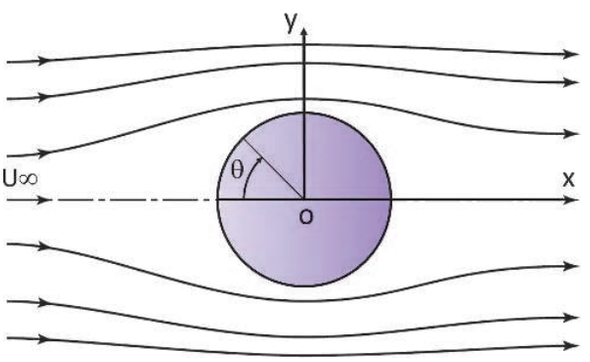

Figure 6.
Potential flow of a cylinder.

The complex potential $w(z)$ corresponding to a cylinder with radius a is given by the superposition of a uniform stream and a doublet [12]

$$w(z) = U_\infty \left(z + \frac{a^2}{z} \right) \tag{29}$$

where z is the complex variable defines as follows:

$$z = x + iy. \tag{30}$$

Real and imaginary parts of w define the potential of velocity ϕ and the stream function ψ, respectively,

$$\phi = U_\infty \left(r + \frac{a^2}{r} \right) cos\theta \tag{31}$$

$$\psi = U_\infty \left(r - \frac{a^2}{r} \right) sin\theta. \tag{32}$$

The conjugate velocity is obtained directly by derivation as follows:

$$\frac{dw}{dz} = U_\infty \left(1 - \frac{a^2}{z^2} \right) = u - iv. \tag{33}$$

This expression can be simplified by making use of the Euler formula $z^{-2} = a^{-2}e^{-i2\theta} = a^{-2}(\,cos\,2\theta - i\ sin\,2\theta)$, and the velocity components over the cylinder surface are the followings:

$$u = 2U_\infty sin^{\,2}\theta \tag{34}$$

$$v = -2U_\infty sin\theta cos\theta. \tag{35}$$

The square of velocity magnitude is given by

$$|V|^2 = u^2 + v^2 \tag{36}$$

$$|V|^2 = U_\infty^2 \left[(1 - \,cos\,2\theta)^2 + (\,sin\,2\theta)^2 \right] \tag{37}$$

$$|V|^2 = 2U_\infty^2 (1 - \,cos\,2\theta). \tag{38}$$

And finally, the modulus of velocity over the cylinder surface is

$$|V| = 2\ U_\infty sin\theta. \tag{39}$$

When the angle is zero, the velocity is zero, corresponding to a stagnation point, but when angle is 90°, the velocity is $2\ U_\infty$, rising to the maximum value of velocity.

The potential flow approximation is valid only in face front the flow, but it is not valid in the wake because the flow is detached. **Figure 7** shows a comparison view between attached flow upstream cylinder (left) and detached flow behind the cylinder (right).

6.3 Boundary layer

Potential flow is used as a first estimation of flow parameters, but it is not a real flow because viscosity is not present in these flow models. The no-slip condition

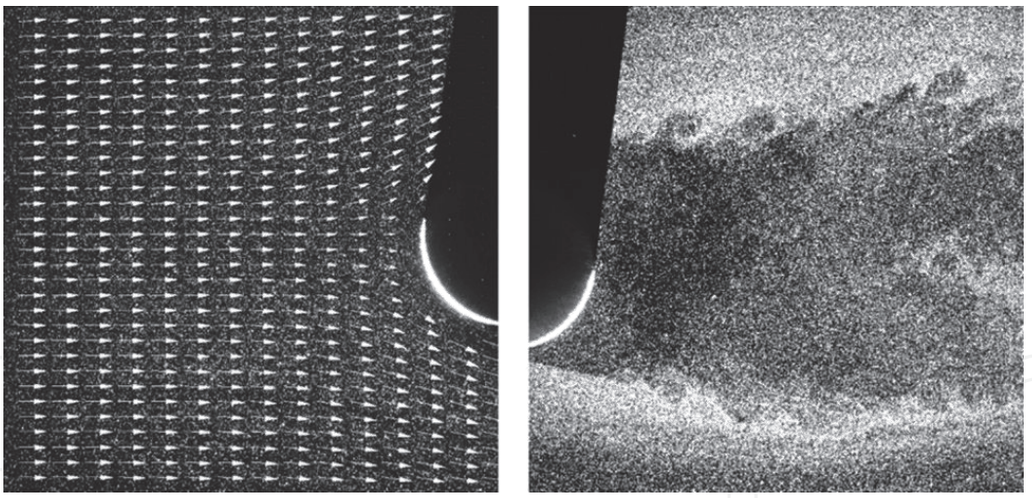

Figure 7.
Real flow around a circular cylinder: Upstream cylinder (left) and behind the cylinder (right).

over the body wall needs zero velocity in the wall and the outer velocity (U_∞) in the boundary layer limit. The boundary layer is a thin layer where the effects of viscous forces are of the same order of the inertial forces. The Reynolds number of flow outer boundary layer is larger than unity, and consequently, the inertial forces are larger than the viscous. When the wind is flowing on the boom surface, the boundary layer is growing downstream and the turbulence and adverse pressure gradients produce the separation of the boundary layer and the detachment of flow, as it can be observed in **Figure 8**. In this situation, wind is flowing over booms in very complex conditions to be simulated analytically and the flow coming to each side of boom depends on the incidence angle of wind, so that thermal sensors are operating in a no ideal condition and heat transfer mechanisms are far from a theoretical environment. It is because the booms are calibrated isolated in order to characterize the output electrical signals from sensor when they are subjected to different wind conditions.

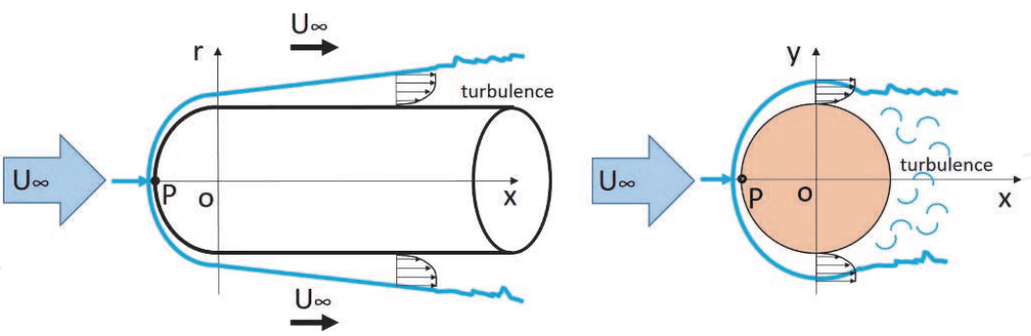

Figure 8.
Boundary layer over the boom.

7. Rover vehicle aerodynamics

The external surface of rover is not designed following aerodynamics criteria. The main body of this vehicle is a box with rectangular section, supported by six wheels. A vertical mast is erected on the upper surface of the main box body. The instruments of MEDA are installed over this mast. Two booms are located perpendicular to the axis mast. The rover vehicle is larger than other elements as mast and booms, and the flow viewed by small devices is mainly affected by the presence of the rover.

The flow visualization is a qualitative technique that offers a global view of the flow so that it provides a first approximation to the study of the flow. **Figure 9** shows the smoke visualization at low Reynolds number when the flow was illuminated by a laser light sheet. This experiment was performed in a small commercial wind tunnel from TSI (model 8390) installed in our laboratory. It was running at an airspeed of 2.6 m/s. This tunnel has a square cross test section of 100×100 mm^2 with transparent walls, in order to provide optical access for the recording camera. The smoke was produced by burning incense bars.

The flow is coming from right to left. Photo in left-hand side shows the streamlines of flow when curved by the presence of the mast and the camera, and a detached flow is produced downstream. On the other hand, photo in right-hand side shows the flow when coming from rear of the rover. The flow is deviated by effects of a large box that corresponds to the module of MMRGT and a detached stream is produced behind this module. Only some streamlines are coming to the camera height but curved.

Figure 10 shows the smoke visualization carried out in the INTA-1 wind tunnel. This facility has maximum airspeed of 60 m/s and closed circuit with open test section of 2×3 m^2. The flow around the rover was running at high Reynolds number and it was illuminated by conventional white light. The flow is steered to the rover presence forming a fine smoke tube, but the direction of the smoke is slightly deflected as it is coming to the rover vehicle rising the boom 1 with an angle different to zero as corresponds to no disturbed horizontal flow, which is the effect of the presence of the rover. The direction of the wind received by sensors is changed by the rover presence. Flow is coming from right to left.

The quantitative analysis of the flow was performed by means of Particle Image Velocimetry (PIV). This is a nonintrusive technique that illuminates the flow seeded with tracer particles and provides simultaneously, the flow field velocity in a plane of the flow [13].

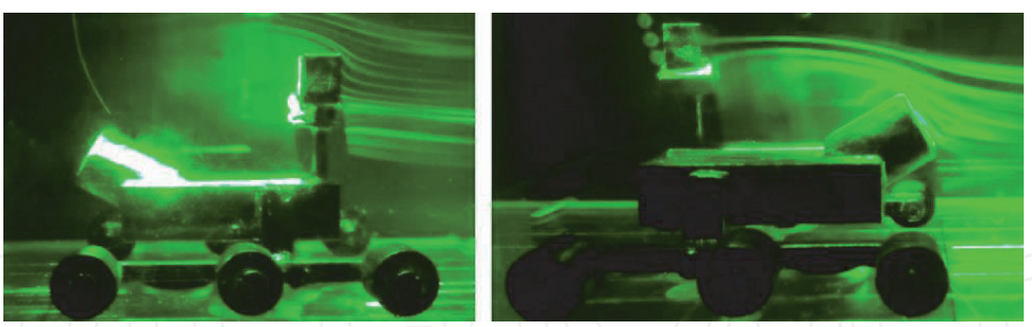

Figure 9.
Smoke visualization of flow around rover (Re = 6770).

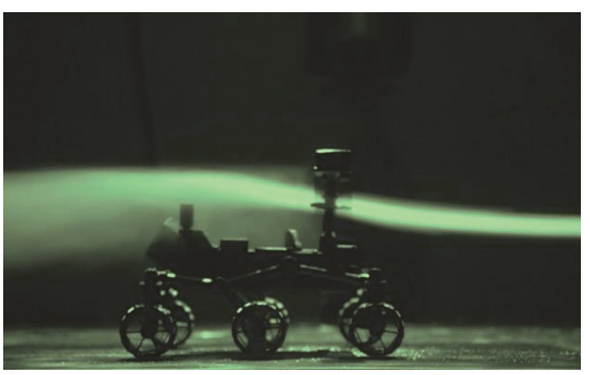

Figure 10.
Smoke visualization of flow around rover (Re = 2.2 × 10^5).

Figure 11 shows the averaged velocity map in a vertical plane of the flow containing the boom 1 of the rover, when the flow was blowing with zero angle of incidence and airspeed of 10 m/s coming from left to right. The color scale represents the velocity magnitude in meter per second. The deflection of streamlines can be observed near the boom 1, although the flow is attached. On the other hand, the flow in the wake of the mast is detached and enclosed in a low-velocity recirculation bubble.

Figure 12 shows the averaged velocity map in a horizontal plane of the flow containing both booms 1 and 2, because they are installed at the same height over the mast. No symmetric deflection of streamlines is observed. This effect is due to the presence of the rover central box and the vertical mast, which is located in the right side of the rover. Flow is coming from left to right and the mast wake is clearly visible, with low velocities (blue color). The wind sensor 2 (WS2) is located as an appendix forming 120° with camera axis.

The flow over the rover was investigated at low Reynolds number (6770) by wind tunnel testing a small rover model with a characteristic length of 38 mm (scale 1: 45th). A TSI model 8390 wind tunnel specially adapted to very low flow velocities was used (mean airspeed of 2.6 m/s). This tunnel has a square cross test section of

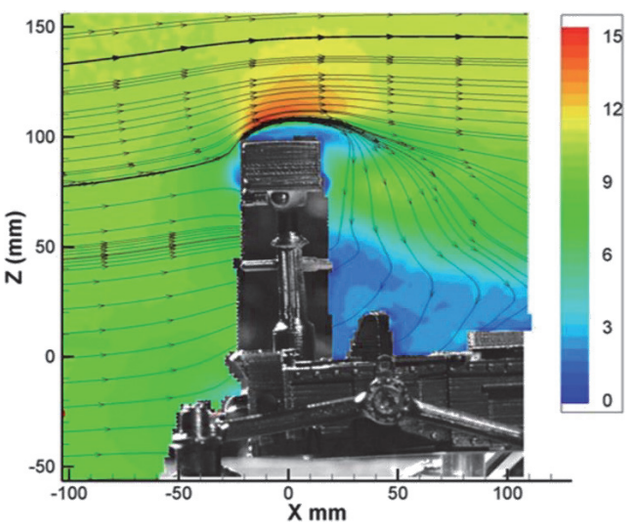

Figure 11.
Velocity map in a vertical plane ($Re = 2.2 \times 10^5$).

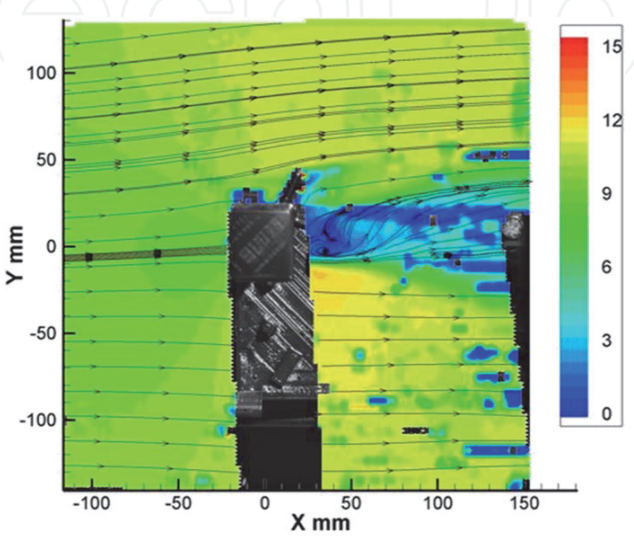

Figure 12.
Top view: Velocity map of a horizontal plane ($Re = 2.2 \times 10^5$).

100×100 mm^2 with transparent walls of methyl methacrylate. It provides optical access for experimental techniques and visual access to the experimentalist.

Laser Doppler Anemometry (LDA) is a punctual nonintrusive measurement technique that is usually used to investigate the flow field velocity with very high accuracy and resolution [14].

Figure 13 shows the experimental set-up, with a body axes system fixed to the model. The angle of wind incidence is defined as β, and the location of both booms is indicated, and the orientation of the LDA probe remains fixed while the model is turning on to simulate different incident wind angles.

LDA measurements were carried out by using a commercial system from Dantec. The illumination source consists of a 10 mW He-Ne laser beam emitting in red color (wavelength of 632.8 nm). A BSA-F60 Flow Processor and BSA Flow software provide data of flow velocity. Seeding particles were produced by means of a water ultrasonic atomizer. **Figure 14** shows the rover model inside the wind tunnel test section during the test experiments and measuring velocity by LDA. Rover vehicle was supported by a circular plate that facilitates the rover turn on during test campaign. Reflexions of red LDA laser beam can be observed in the walls of wind tunnel test chamber.

Modulus of wind velocity in sensor 1 location is determined from three orthogonal velocity components measured by LDA after the following expression:

$$V_1 = \sqrt{U_{LDA}^2 + V_{LDA}^2 + W_{LDA}^2}. \tag{40}$$

An analogous expression was used to compute the velocity at the location of sensor 2.

Figure 15 shows the modulus of velocity as seen by both wind sensors WS1 and WS2. Differences with freestream velocity are observed in wind velocity detected by laser Doppler in respective locations of rover wind sensors. Velocities were measured for different incidence wind angles in range 0–360°. Two forbidden bands that correspond to not valid data are marked in **Figure 15**. These areas correspond to detached flow when the sensors are located mainly in the wake of camera mast and MMRGT of rover. In practice, the solution is to use active operating redundancy, since both sensors are operating simultaneously in order to complement the forbidden regions, so that whole angular sector can be measured by rover sensors.

The sensor 1 (WS1) is the main sensor because this sensor will be used for wind measurements except in the not valid region. The sensor 2, named as WS2, must be used in the forbidden band of sensor 1.

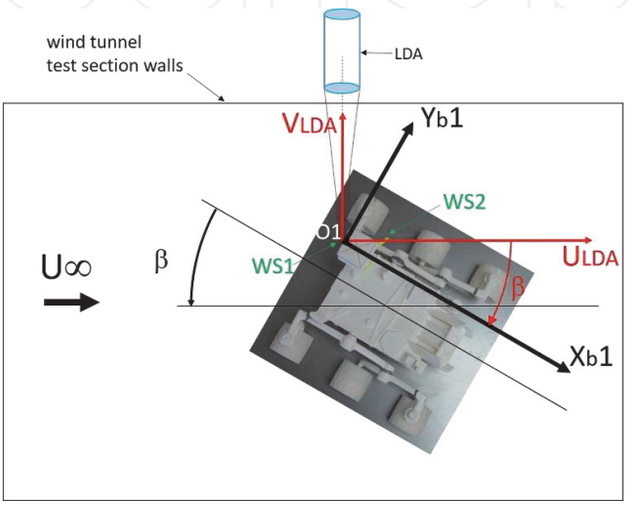

Figure 13.
Top view: Velocity map of a horizontal.

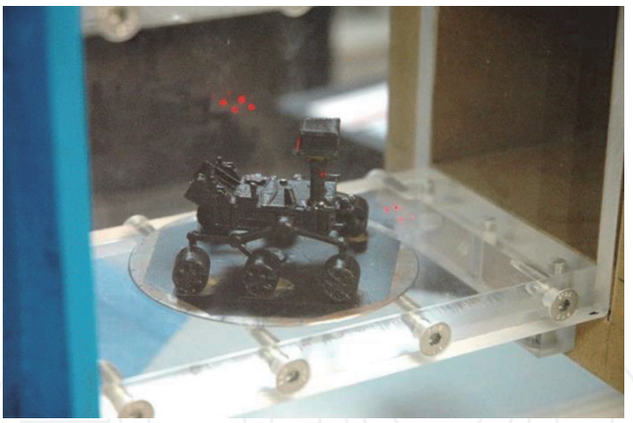

Figure 14.
Rover model inside the test section during LDA measurements.

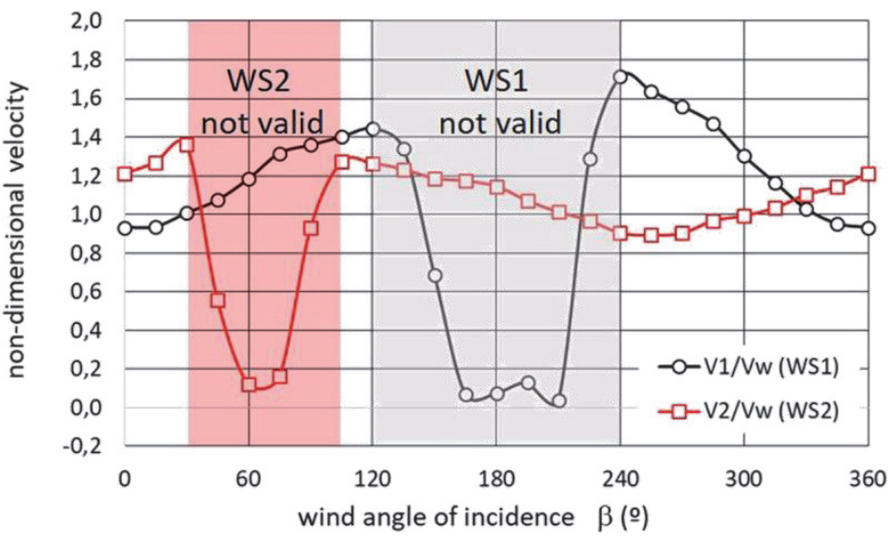

Figure 15.
Wind velocity measured by rover booms.

On the other hand, measurements provided by both sensors in the cut-off angles (30, 105, 120, and 240°) are valid, and the wind velocity in these points would be determined by an averaged velocity value.

Figure 16 shows forbidden circular sectors for both wind sensors measurements. When wind is blowing from forbidden angles of incidence, the flow is detached by a combined effect of the camera mast and MMRGT of rover that produce a turbulence flow in the mast wake that is coming to the booms where the rover wind sensors are installed. Graphs in **Figure 16** demonstrate that complete circular angles range can be measured by the combination of both wind sensors.

Finally, the velocity measured by each wind sensor must be corrected from the effects of the external geometry of the rover vehicle. The true wind velocity V_W is given by

$$V_W = K_i V_i; i = 1, 2 \tag{41}$$

where K_i is the calibration factor that must be determined for each sensor, from data contained in **Figure 15**, by computing calibration factors by the following expression:

$$K_i = \frac{V_W}{V_i}. \tag{42}$$

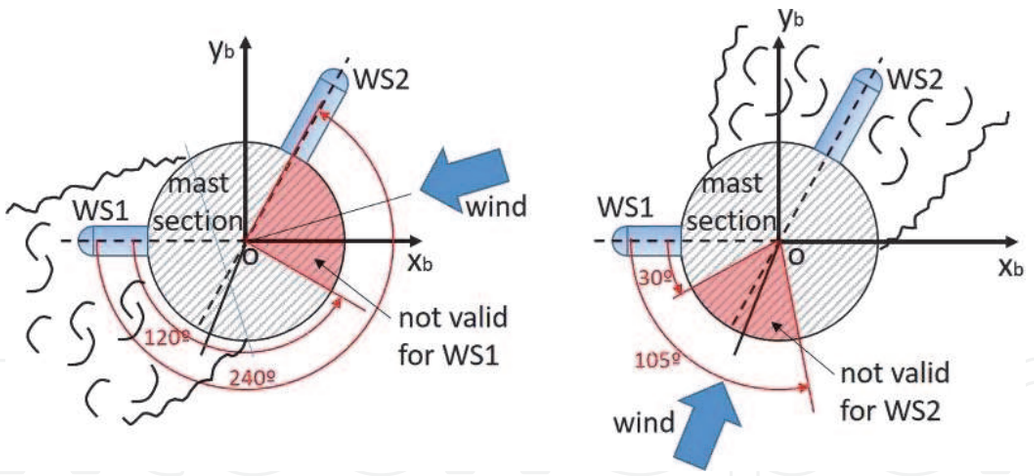

Figure 16.
Forbidden circular sectors for wind sensors measurements.

This ratio is precisely the inverse of this presented in **Figure 15** and it represents the effect of rover vehicle over the booms.

8. Conclusions

The Mars 2020 rover aerodynamics plays a fundamental role in the operation of rover wind sensors. A set of hot film sensors have been specially designed to be installed over two booms located perpendicular to camera mast of rover. This kind of sensors are based on the heat transfer from sensors to environment around the sensors, but physical properties of Earth atmosphere are very different to these present in Mars atmosphere where sensors will operate during Mars 2020 mission.

Reynolds number is the fundamental parameter to establish the physical similarity between real flow in Mars and this investigated in Earth by wind tunnel testing.

Potential flow provides a first approximation to study the longitudinal and transversal flows over booms where wind sensors will be installed. Limitations of the potential model are evidenced by detachment flow in the wake of booms with transversal flow and the presence of the boundary layer where viscous effects are of the same order of inertial effects. Due to these limitations, a more intensive experimental investigation is necessary. Global information about the flow pattern around the rover vehicle was obtained by smoke visualization. Qualitative techniques as Particle Image Velocimetry (PIV) and Laser Doppler Anemometry (LDA) were used to get insight about the velocity field. The effects of rover vehicle over the flow coming to the sensors booms were studied, and not valid regions of each sensor were determined.

Finally, the calibration factor equation was indicated as the main way to correct flow velocity from the adverse effects produced by the rover vehicle over wind sensors measurements.

Acknowledgements

This investigation was funded by Spanish Ministry of Defense under the program “IGB 99001 Termofluidodinámica” of INTA (National Institute for Aerospace Technology of Spain).

Nomenclature

A	transversal area of body boom
A_w	area of heat transfer for the wire
a	radius of the boom
C	empirical coefficient
C_1	empirical coefficient
D	empirical coefficient
D_1	empirical coefficient
d	wire diameter
E	energy of wire
E_W^2	voltage of the wire
g	gravity
h	thermal convection coefficient
I	electric intensity crossing the wire
k	conductivity of fluid
K_i	calibration factor of velocity
Kn	Knudsen number
L	characteristic length scale
M	strength of a three-dimensional point source
n	empirical coefficient
Nu	nondimensional Nusselt number
Q	transferred heat to the flow
R	electric resistance of the wire
Re	Reynolds number
$RCO2$	constant of CO2 gas
R_g	constant of gas fluid
S	reference temperature
T_w	wire temperature
T_∞	flow temperature
u	flow velocity component
U_∞	freestream velocity
U_{LDA}	velocity component measured by LDA after x axis of rover
v	flow velocity component
V	flow velocity
$\|V\|$	modulus of velocity
V_{LDA}	velocity component measured by LDA after y axis of rover
V_W	true wind velocity
V_1	wind velocity measured in location of boom 1.
W	heating power of wire
W_{LDA}	velocity component measured by LDA after z axis of rover

Greek symbols

λ	mean free path
ρ	density
Φ	velocity potential
μ	dynamic viscosity coefficient of the fluid
ν	kinematic viscosity coefficient of the fluid
Ψ	stream function

Author details

Rafael Bardera*, Suthyvann Sor and Adelaida García-Magariño
National Institute for Aerospace Technology, Madrid, Spain

*Address all correspondence to: barderar@inta.es

IntechOpen

References

[1] Tahu G. Environmental Impact Statement for the Mars 2020 Mission. NASA Reptort 20546; Washington, D.C.; 2014

[2] Gómez-Elvira J, REMS Team. Environmental monitoring instrument for Mars exploration. Lunar and Planetary Science. March 10-14, 2008. pp. 1647-1648

[3] Gómez-Elvira J et al. REMS: The environmental sensor suite for the Mars science laboratory rover. Space Science Reviews. 2012;**170**:583-640. Springer

[4] Domínguez M, Jiménez V, Ricart J, Kowalski L, Torres J, Navarro S, et al. A Hot Film Anemometer for the Martian Atmosphere. Planetary and Space Science. USA: Elsevier; 2008. pp. 1169-1179

[5] Petrosyan A, et al. The Martian Atmospheric Boundary Layer, Reviews of Geophysics, 49, RG-3005/2011. American Geophysics Union

[6] Leovy CB. Martian meteorology. Annual Review of Astronomy and Astrophysics. 1979;**17**:387-413. Annual reviews Inc

[7] Schetz JA, Fuhs AE. Chapter 11: Rarified gas dynamics. In: Handbook of Fluid Dynamics and Fluid Machinery. USA: John Wiley & Sons, Inc; 1996. p. 672

[8] White F. Fluid Mechanics. Fourth ed. Boston, Massachusetts, USA: McGraw-Hill Companies, Inc.; 2002

[9] Bhandari P, Anderson K. CFD analysis for assessing the effect of wind on the thermal control of the Mars Science Laboratory Curiosity Rover. In: International Conference on Environmental Systems (ICES). AIAA, Vail, CO; 2013

[10] Chamberlain TE. Atmospheric measurements on Mars: The Viking meteorology experiment. Bulletin American Meteorological Society. 1976; **57**(9):1094-1104

[11] Hess SL, Henry RM, Kuettner J, Leovy CB, Ryan JA. Meteorology Experiments: The Viking Mars Lander, Icarus. Vol. 16. USA: Elsevier, Inc.; 1972. pp. 196-204

[12] Kundu PK, Cohen IM. Fluid Mechanics. Second ed. USA: Elsevier Science; 2002. pp. 160-163

[13] Raffel M, Willert CE, Wereley ST, Kompenhans J. Particle Image Velocimetry: A Practical Guide. Berlin, Heidelberg, Germany: Springer-Verlag; 2007

[14] Albrech HE, Borys M, Damaschke N, Tropea C. Laser Doppler and Phase Doppler Measurement Techniques. New York, NY, USA: Springer; 2003